A multiscale analysis in CD38 −/− mice unveils major prefrontal cortex dysfunctions

Lora L Martucci, Muriel Amar, Rémi Chaussenot, Gabriel Benet, Oscar Bauer, Antoine de Zélicourt, Anne Nosjean, Jean-Marie Launay, Jacques Callebert, Catherine Sebrié, et al.

THE FASEB JOURNAL • RESEARCH • www.fasebj.org

A multiscale analysis in CD38$^{-/-}$ mice unveils major prefrontal cortex dysfunctions

Lora L. Martucci,[*,†,1] Muriel Amar,[*,1] Remi Chaussenot,[*] Gabriel Benet,[*] Oscar Bauer,[*,‡] Antoine de Zélicourt,[*,†] Anne Nosjean,[*] Jean-Marie Launay,[§] Jacques Callebert,[§] Catherine Sebrié,[¶] Antony Galione,[‖] Jean-Marc Edeline,[*] Sabine de la Porte,[†] Philippe Fossier,[*] Sylvie Granon,[*] Cyrille Vaillend,[*] and José-Manuel Cancela[*,2]

[*]Neuroscience Paris–Saclay Institute (Neuro–PSI), Unité Mixte de Recherche (UMR) 9197, and [¶]Imagerie par Résonance Magnétique Médicale et Multimodalité (IR4M) UMR 8081, Paris-Sud University, Paris–Saclay University, CNRS, Orsay, France; [†]INSERM U1179, Handicap Neuromusculaire: Physiologie, Biothérapie et Pharmacologie Appliquées, Unité de Formation et de Recherche (UFR) des Sciences de la Santé Simone Veil, Université de Versailles Saint-Quentin-en-Yvelines (UVSQ), Montigny-le-Bretonneux, France; [‡]Génétique Humaine et Fonctions Cognitives, UMR 3571, Gènes, Synapses et Cognition, CNRS, Institut Pasteur, Paris, France; [§]Unité 942, Hôpital Lariboisière, INSERM, Paris, France; and [‖]Department of Pharmacology, University of Oxford, Oxford, United Kingdom

ABSTRACT: Autism spectrum disorder (ASD) is characterized by early onset of behavioral and cognitive alterations. Low plasma levels of oxytocin (OT) have also been found in ASD patients; recently, a critical role for the enzyme CD38 in the regulation of OT release was demonstrated. CD38 is important in regulating several Ca^{2+}-dependent pathways, but beyond its role in regulating OT secretion, it is not known whether a deficit in CD38 expression leads to functional modifications of the prefrontal cortex (PFC), a structure involved in social behavior. Here, we report that CD38$^{-/-}$ male mice show an abnormal cortex development, an excitation-inhibition balance shifted toward a higher excitation, and impaired synaptic plasticity in the PFC such as those observed in various mouse models of ASD. We also show that a lack of CD38 alters social behavior and emotional responses. Finally, examining neuromodulators known to control behavioral flexibility, we found elevated monoamine levels in the PFC of CD38$^{-/-}$ adult mice. Overall, our study unveiled major changes in PFC physiologic mechanisms and provides new evidence that the CD38$^{-/-}$ mouse could be a relevant model to study pathophysiological brain mechanisms of mental disorders such as ASD.—Martucci, L. L., Amar, M., Chaussenot, R., Benet, G., Bauer, O., de Zélicourt, A., Nosjean, A., Launay, J.-M., Callebert, J., Sebrié, C., Galione, A., Edeline, J.-M., de la Porte, S., Fossier, P., Granon, S., Vaillend, C., Cancela, J.-M., A multiscale analysis in CD38$^{-/-}$ mice unveils major prefrontal cortex dysfunctions. FASEB J. 33, 000–000 (2019). www.fasebj.org

KEY WORDS: behavior · oxytocin · autism · monoamines · excitation

Autism spectrum disorder (ASD) covers a group of neurodevelopmental disorders characterized by behavioral and cognitive disturbances with early-onset deficits in language acquisition and social interaction. ASD is highly inherited but the genetic determinants are poorly understood. The genetic basis of ASD has been associated with copy-number variations or single-nucleotide polymorphism (SNP) in genes involved in brain development, synapse formation, or cell signaling (1). ASD is frequently associated with excessive cortical growth (2), and a current hypothesis is that the behavioral defects observed in ASD are due to impairments in synaptic functioning and plasticity (1, 3–5). For example, some mutations affect glutamatergic synaptic transmission such as for the SH3 and multiple ankyrin repeat domain (SHANK) proteins (4–6) or the neuroligins (3, 7). One important consequence of these mutations is that the mechanisms of synaptic plasticity are altered and affect ionotropic NMDA receptors or metabotropic glutamate receptors regulating learning processes and cognitive functions (8, 9). Recently, the hypothesis of an increase in the excitation-inhibition (E-I) ratio in neuronal circuits emerged as a common pathophysiological principle that could explain the genesis of cognitive and social behavior deficits in ASD (10).

ABBREVIATIONS: 5-HIAA, 5-hydroxyindoleacetic acid; 5-HT, serotonin; ABR, auditory brainstem response; ASD, autism spectrum disorder; CS, conditioned stimulus; DA, dopamine; dB, decibel; E-I, excitation-inhibition; HFS, high-frequency stimulation; L5PyN, pyramidal neuron of layer 5; LTP, long-term potentiation; MΩ, megaohm; mPFC, medial PFC; NE, norepinephrine; OT, oxytocin; PFC, prefrontal cortex; SHANK, SH3 and multiple ankyrin repeat domain; SNP, single-nucleotide polymorphism; UCS, unconditioned stimulus; USV, ultrasonic vocalization

[1] These authors contributed equally to this work.

[2] Correspondence: Neuroscience Paris-Saclay Institute (Neuro-PSI) CNRS UMR 9197, Paris-Sud University, Paris-Saclay University, Claude Bernard, 91405 Orsay, France. E-mail: jose-manuel.cancela@u-psud.fr

doi: 10.1096/fj.201800489R

This article includes supplemental data. Please visit *http://www.fasebj.org* to obtain this information.

Remarkably, experimental perturbation of the E-I balance in the prefrontal cortex (PFC) of mice reproduces autistic-like behavioral defects and therefore supports this hypothesis (11). Some mouse models of ASD have changes in the E-I balance in favor of a greater excitation (1, 10, 12–14). Recently, oxytocin (OT) has been shown to play a crucial role in synapse maturation and in synaptic transmission (14–17).

Several studies have pointed toward a deficit in OT signaling in patients with ASD (18–22). Low plasma levels of OT have been found in ASD patients and, although a deficit in OT may not be a primary cause in ASD cases, several studies have suggested that such deficits likely contribute and worsen the social deficit observed in these patients (18, 21–24). The enzyme CD38, known for catalyzing the production of second messengers upon GPCRs (25–28), is an important player in social behavior and is one of the major signaling components controlling the Ca^{2+}-dependent secretion of OT (29, 30). Moreover, CD38 has been associated with familial forms of ASD with a common SNP (CD38 rs3796863) (21).

Identifying if and how genetic defects associated with ASD alter the E-I balance of the PFC, cognitive functions, and social behavior constitutes an important challenge in the search of common therapeutic targets for this neurodevelopmental disorder. Considering that in patients the risk factor SNP, CD38 rs3796863, results in low expression of CD38 and low plasma levels of OT, we focused our present study on $CD38^{-/-}$ mice to determine whether CD38 loss of function, which reduces OT secretion, affects brain development, E-I balance, and plasticity of the PFC, as well as cognitive, emotional, and social processes. In the present study, we report that $CD38^{-/-}$ mice display macrocephaly and larger cortical layers, a shift of the E-I balance toward higher excitation, impaired synaptic plasticity, and altered monoamine levels in the PFC. This is associated with enhanced anxiety-like responses, altered vocal communication, and social behavior with enhanced aggressiveness during social interactions.

MATERIALS AND METHODS

Animals

Male C57BL/6 mice (CD38 sufficient) were purchased from Janvier Labs (Le Genest-Saint-Isle, France). $CD38^{-/-}$ mice holding a deletion of exon 2 and 3 in the CD38 gene were obtained from the Lund and Randall Laboratory [University of Alabama–Birmingham (UAB), AL, USA]. The $CD38^{-/-}$ mice have been backcrossed 10 times onto the C57BL/6 inbred strain background and were shown to exhibit no residual enzymatic activity *in vitro* (31). The $CD38^{-/-}$ mice received from the Lund and Randall Laboratory were crossed on a regular basis with C57BL/6 mice to generate our colony. For genotyping, genomic DNA was isolated from mice tails using the Nucleospin Tissue Kit (Macherey Nagel, Bethlehem, PA, USA). Exon 2 was amplified by PCR and products were analyzed in agarose gel electrophoresis. C57BL/6 mice and $CD38^{-/-}$ mice were bred in our animal facility at the Neuroscience Paris-Saclay Institute. For behavioral studies, adult mice were >3 mo old and juvenile mice were postnatal day (P)28–P30 d old. For each behavioral experiment, the apparatus was gently washed before each animal testing. Animal care and experimental procedures complied with the European Communities Council Directive (CEE 86/609/EEC), European Union Directive 2010/63/EU, and the local ethics committee (Paris Centre et Sud, N°59).

Magnetic resonance imaging

Mice were imaged under isoflurane anesthesia (induction 2%; flow rate 0.8 in 50% O_2, 50% N_2O) and controlled on the basis of respiratory parameters. The body temperature was maintained at 37°C using a heated mattress. MRI measurements were performed on a 7 T horizontal bore magnet driven by Paravision and equipped with a 300 mT/m actively shielded gradient device with the internal diameter = 90 mm (Bruker, Billerica, MA, USA). For MRI examination, the animal's head was introduced in a "bird-cage" [^{1}H] coil (internal diameter = 22 mm). The mouse brain was positioned using scouting gradient-echo images in the 3 orthogonal directions. After the shimming process, 3 Turbo-Rapid Acquisition with Relaxation Enhancement (Turbo-RARE) sequences with fat suppression were acquired: 1 perpendicular (axial) to the brain anteroposterior axis (repetition time/effective echo time = 5000/40 ms ; rare factor = 8; 2 averages; 37 contiguous 0.5-mm thick sections; 20 × 20 mm field of view; 256 × 256 matrix; pixel size = 78 μm^2) and 2 parallel (coronal and sagittal) to the brain anteroposterior axis [repetition time/effective echo time = 5000/40 ms; rare factor = 4; 2 averages; 40 × 20 mm field of view; 512 × 256 matrix; voxel size = 78 μm^2 and respectively 43 (sagittal MRI) and 35 (coronal MRI) contiguous 0.25-mm–thick sections]. The total time spent by the mouse in the magnet was around 25 min. After each experiment, mice were released from anesthesia and returned to their home cages with free access to food and water.

Slice preparation and electrophysiological recordings

Coronal slices (250 μm thickness) of the PFC were obtained from P21 to P28 male mice. They were incubated for at least 1 h at 33°C in an extracellular solution containing the following (in millimolars): NaCl, 126; $NaHCO_3$, 26; glucose, 10; $CaCl_2$, 2; KCl, 1.5; KH_2PO_4, 1.25; $MgCl_2$, 2 (pH 7.4, 310–330 mosmol) and oxygenated continuously with a mixture of 95% O_2 and 5% CO_2. Electrical stimulations (1–10 μA, 0.2 ms duration) were delivered in layer 2–3 using 1 megaohm (MΩ) impedance bipolar tungsten electrodes (TST33A10KT; WPI). The intensity of the stimulation corresponded to 50% of the maximum response. Somatic whole-cell recordings were performed in pyramidal neurons of layer 5 (L5PyNs) at 33°C using borosilicate glass pipettes (3–5 MΩ resistance in bath) filled with a solution containing the following (mM): K-gluconate, 140; HEPES, 10; ATP, 4; $MgCl_2$, 2; GTP, 0.4; EGTA, 0.5 (pH 7.3 adjusted with KOH; 270–290 mosmol). Voltage-clamp recordings were performed using an Axoclamp-2A (Molecular Devices, San Jose, CA, USA), filtered by a low-pass Bessel filter with a cutoff frequency set at 2 kHz, and digitally sampled at 4 kHz. The membrane potential was corrected offline by −10 mV to account for junction potential. The firing profile of patched neurons and their membrane resistance were obtained using 1 s depolarizing steps ranging from −100 to 200 pA. Only cells having a resting membrane potential more negative than −55 mV and with an access resistance lower than 25 MΩ were kept for further analysis. The access resistance was compensated offline in voltage-clamp mode and neurons exhibiting >10% of access resistance were rejected. Analysis of the synaptic response and decomposition of synaptic conductance changes were performed as extensively described in previous publications (32–37).

Synaptic plasticity

A high-frequency stimulation (HFS) protocol was applied in the PFC layer 2–3 with θ-burst stimulation (3 trains of 13 bursts at

5 Hz, each burst containing 4 pulses at 100 Hz, for a total duration of 2 min), whereas the L5PyN was under the current clamp condition. Recordings of current responses in L5PyNs were then done as previously described (frequency of stimulation 0.05 Hz) at 15, 30, 45, and 60 min after the beginning of the HFS protocol for comparison with control recordings. Changes above 20% of control conductance before the HFS protocol were considered as reflecting long-term potentiation (LTP), a long-lasting enhancement of neurotransmission that could be blocked by an NMDA-receptor antagonist (D-L-AP5, unpublished results), thus demonstrating that LTP depended on activation of these receptors in our experimental conditions.

Social interaction task

The social interaction task was previously described in detail by Granon *et al.* (38). Briefly, it took place in an in-laboratory made transparent Plexiglas cage (50 cm long × 25 cm wide × 30 cm deep) located in a nonfamiliar experimental room with a 100 lux illumination. It contained a handful of clean sawdust for each mouse. The experimental cage was located below a camera connected to a computer that recorded video of social behavior for subsequent offline analyses. One mouse, either of the $CD38^{-/-}$ or C57BL/6 genotype, was placed alone in the experimental cage and was allowed to freely explore for 30 min. A novel mouse (same gender, age, weight, and C57BL/6 genotype) was then gently introduced in the cage for an 8-min test during which we recorded ultrasonic vocalizations (USVs). For the experiment with juvenile mice, the experimental design is identical to the one described above for the adult mice except that the novel mouse is from the same genotype of the tested mouse. Multiple social parameters were analyzed offline, such as the duration of contact between the 2 mice and the number of aggressive attacks. Adult male mice were isolated 3 wk before testing, whereas juveniles were not.

USV recording

USVs were recorded during the social interaction task in dyads of mice (39). A condenser ultrasound microphone Polaroid/CMPA (Avisoft Bioacoustics, Berlin, Germany) was placed high enough above the experimental chamber so that the receiving angle of the microphone covered the whole area of the test cage. It was connected to an ultrasound recording interface (UltraSoundGate 416H; Avisoft Bioacoustics) plugged to a computer equipped with the Avisoft Recorder USG (sampling frequency: 250 kHz; FFT-length: 1024 points; 16-bit format; Avisoft Bioacoustics). Spectrograms were generated for each detected call to measure the number of calls and their duration (39, 40) with the following characteristics: Blackman window, overlap: 87.5%, time resolution: 0.512 ms, frequency resolution 244 Hz.

Three-chamber social behavior test

In the first part of the test, a C57BL/6 or $CD38^{-/-}$ mouse was placed in the 3-chambered apparatus (transparent Plexiglas cage separated in 3 different and accessible rooms and was allowed to freely explore the environment for 10 min (habituation period). Then, the mouse was put back in its home cage for 1 min. A "stranger" C57BL/6 mouse was placed in 1 of the 2 cups (the social cup) and the other remaining empty cup was called the "unknown object" (or nonsocial cup). In the second part, the tested C57BL/6 or $CD38^{-/-}$ mouse was placed in the center zone and allowed to explore all chambers for 10 min (social motivation test). Contacts were scored when the mouse sniffed and touched the unknown object or the social cup. The experimental apparatus was located in a room under 100 lux illumination and below a camera connected to a computer for video recording of social behavior for subsequent offline analyses (AnyMaze, Wood Dale, IL, USA).

Light–dark choice anxiety test

The apparatus had 20-cm high Plexiglas walls and consisted of a brightly lit white compartment (40 × 15 cm; illumination: 600 lux) connected by a trap door (6 × 6 cm) to a dark compartment (15 × 15 cm; illumination <10 lux). Each mouse was placed in the dark compartment for 20 s; the trap door was then opened and mice were allowed to freely explore the whole apparatus for 5 min. Step-through latency, the number of entries, and total time spent in the lit compartment were scored.

Elevated plus-maze anxiety test

The maze had 2 facing arms enclosed with high walls (20 × 8 × 25 cm), 2 open arms (20 × 8 cm) and a central area (8 × 8 cm) forming a plus sign 65 cm above the floor. Illumination was 140 lux in open arms and 30 lux in enclosed arms. Mice were individually placed at the center of the maze with the head facing an open arm. The number of entries and time spent in open or enclosed arms were recorded for 5 min. Head-dipping over sides of open arms were counted and classified as protected head dips when the rest of the mouse's body remained in a closed arm, and as unprotected head dips when the whole mouse's body was located in the open arm.

Open-field exploratory activity

The test box was a square open field (50 × 50 × 50 cm) with black walls and a white floor under homogeneous illumination (100 lux in center area). Each mouse was released near the wall and tracked by video for 40 min using the AnyMaze software. Recorded *x-y* positions were used to generate a tracking plot of the exploration paths and to calculate the distance traveled, speed, and time spent in distinct zones of the box [*i.e.*, in the whole apparatus, in a virtual corridor (width: 10 cm) along the walls, and in the remaining central area, referred to as the center area]. Latency of the first entry, the number of entries, and the percent distance traveled in center area and along walls were calculated as relative measures of anxiety.

Contextual fear conditioning

The conditioning box consisted of a grid floor (30 × 30 cm) enabling delivery of electric foot shocks as unconditioned stimuli (UCS) and clear Plexiglas walls (45 cm in height) with no ceiling in order to allow full observation and video tracking. Experiments were performed under moderate illumination (150 lux). During acquisition (d 1, duration: 8 min), each mouse was allowed to freely explore the box for 2 min; 3 foot shocks (0.4 mA, 2 s) were then successively delivered with a 2-min interval between shocks (2, 4, 6 min), and the mouse remained in the box for 2 min after the last shock. Retention and extinction of conditioned fear was measured during the next 3 d (24, 48, 72 h) by placing the mouse in the same context for 20 min during each daily session without any foot shock. Tonic immobility (freezing) was analyzed from video-tracking plots (AnyMaze) and used to quantify expression of fear responses and fear memory.

Auditory-cued fear conditioning

Conditioning procedure was performed using the StartFear system (Panlab, Barcelona, Spain). The conditioning chamber

(25 × 25 × 25 cm) had 3 black methacrylate walls, a transparent front door, a grid floor connected to a shock (UCS) scrambler and a speaker on the ceiling to deliver audible tones as conditioned stimuli (CS). It stood on a high-sensitivity weight transducer system generating analogical signals reflecting the animal's movement and was confined in a ventilated soundproof enclosure on an antivibration table with surrounding 60-decibel (dB) white noise. Interchangeable floors and walls were used to analyze fear memory in a novel context. On the first day (acquisition), a 2-min baseline period was recorded before delivery of 3 CS-UCS pairs (tone: 80 dB, 10 kHz, 30 s; foot shocks: each at 0.2 mA for 2 s). On the next day (retention), the mouse was placed in a different context for 2 min (baseline) before delivery of 4 CS (80 dB, 10 kHz, 30 s). In both sessions, stimuli were separated by pseudorandomly distributed intervals (60–180 s). The animal's movements were sampled at 50 Hz for quantitative analysis (Freezing software; Panlab). Freezing was analyzed during delivery of the CS (periods of 30 s) to specifically reflect associative learning performance.

Auditory brainstem responses

Thresholds for the averaged auditory brainstem response (ABR) were used here as an electrophysiological measure of auditory sensitivity (41, 42). ABRs were recorded in response to acoustic stimuli under deep anesthesia (95 mg/kg ketamine, 24 mg/kg xylazine, i.p.). Mice were placed on a heating blanket to avoid hypothermia. Auditory stimuli were presented monaurally using an insert earphone (Etymotic Research, Elk Grove Village, IL, USA) ending with a 17-mm polyethylene tubing inserted into external auditory meatus to avoid sound reverberation on the ear lobe. ABRs were recorded using 2 subcutaneous electrodes (SC25; Neuroservice, Aix-en-Provence, France) located just above the tympanic bulla and skull dorsal midline and 1 ground electrode placed in the thigh. Insertion of subcutaneous electrodes was not associated with any sign of discomfort. ABRs were collected by a Centor-USB interface (DeltaMed, Friedberg, Germany). Pure tone bursts (duration: 10 ms; rise-fall time: 2 ms) were delivered at specific frequencies (8, 2, 16, 24, 4, and 32 kHz) and presented at 70, 50, 40, 30, 20, 10, 5, and 0 dB sound pressure level. Stimuli were presented at 15 Hz. The signal was filtered at 0.2–3.2 kHz with a sampling rate of 100 kHz, and waveforms were averaged (500–1000 waveforms depending on the stimulus intensity) and stored for offline analyses. All sound intensities are expressed in dB sound pressure level.

Acoustic startle reflex and auditory gating

Testing was conducted in the same conditioning chamber used for auditory-cued fear conditioning. Mice were individually placed in a small nonrestraining Plexiglas cylinder (5 × 10 × 3.5 cm) mounted on the grid floor 5 min prior to testing (acclimation period) and throughout the experiment. A background white noise (65 dB) was present throughout testing. The acoustic startle reflex was detected by a piezoelectric accelerometer plugged to the grid floor and evaluated in response to 4 blocks of 9 startling tones (pulses of 70, 80, 90, 95, 100, 105, 110, 115, and 120 dB; 10 kHz, 40 ms) presented in a pseudorandom order with intertrial intervals of 10, 15, or 20 s. In a second experiment (24 h later), the maximal startle amplitude induced by 120 dB pulses was modulated by the presentation of non-startling low-intensity prepulses [68–77 dB (*i.e.*, 0–12 dB above background noise), 10 kHz, 20 ms] pseudorandomly delivered 100 ms before the 120 dB startling pulse [prepulse inhibition (PPI)]. In both experiments, individual amplitudes recorded in distinct blocks of trials were averaged. PPI was normalized to the startle amplitude induced by the 120 dB startling pulses.

Plasma OT levels measurement

Mouse blood samples were centrifuged (5 min, 5000 rpm, 4°C), and plasma samples (50 μl) were kept at −20°C until the extraction step performed at 4°C as follows: 20 mg of heat-activated (700°C) LiChroprep Si 60 (Merck, Darmstadt, Germany) in 1 ml distilled water was added to each sample, mixed for 30 min, and centrifuged; the pellet was mixed in 60% acetone to elude the neuropeptide; the evaporated extracts were kept at −20°C. The plasma OT content was estimated using a highly sensitive and specific radioimmunoassay (RIAgnosis, Munich, Germany) (43, 44). In brief, 0.05 ml of rabbit anti-OT antibody was applied for 60 min and 0.01 ml of [^{125}I]-labeled tracer (PerkinElmer, Waltham, MA, USA) were then added to each aliquot. After an incubation period of 3 d at 4°C, unbound radioactivity was precipitated by activated charcoal (MilliporeSigma, Burlington, MA, USA).

Measurements of monoamines and associated metabolites

Amounts of norepinephrine (NE), serotonin (5-HT) dopamine (DA) and their metabolites were quantified by ultra performance liquid chromatography. Briefly, the PFC was quickly removed and homogenized in 0.3 M perchloric acid and centrifuged at 22,000 *g* for 30 min at 4°C. Supernatants were collected and filtered through a 10 kDa membrane (Nanosep; Pall, Port Washington, NY, USA). Then 50 μl of each sample was analyzed through a 4-channel electrochemical array detector (Thermo Fisher Scientific, Waltham, MA, USA). Analysis, data collection, and peak identification were fully automated (Chromeleon 7; Thermo Fisher Scientific). The results were expressed as femtomoles per milligram of fresh tissue.

Statistical analysis

Normality was tested with the Kolmogorov-Smirnov test and the d'Agostino and Pearson test. When data did not follow a normal distribution, we used the Mann-Whitney 2-tailed nonparametric test. For multiple comparison, 2-way ANOVA was used. Each value is expressed as means ± SEM. Values of $P<0.05$ were considered significant.

RESULTS

Brain morphologic alterations

We examined whether adult CD38$^{-/-}$ male mice could exhibit abnormal cortical development knowing that CD38 plays a critical role in cell differentiation. We performed *in vivo* MRI to assess volumetric estimation of different brain structures in CD38$^{-/-}$ mice. **Figure 1** shows MRI evaluation of brain volumetric integrity with images corresponding to both 2-dimensional cutting plane (Fig. 1*A*) and 3-dimensional reconstruction of mouse brains (Fig. 1*B–D*). The whole brain volume was significantly larger in CD38$^{-/-}$ mice compared with C57BL/6 mice (Fig. 1*E*, 551.7 ± 5.2 mm^3 for CD38$^{-/-}$ *vs.* 527.2 ± 4.9 mm^3 in control mice). Volumes of different structures were analyzed, and we found that the cortex and ventricles were significantly larger in CD38$^{-/-}$ mice compared with C57BL/6 mice (Fig. 1*E*, Cortex: 189.1 ± 2.1 mm^3 for CD38$^{-/-}$ mice *vs.* 181.1 ± 2.0 mm^3 for controls; ventricles:

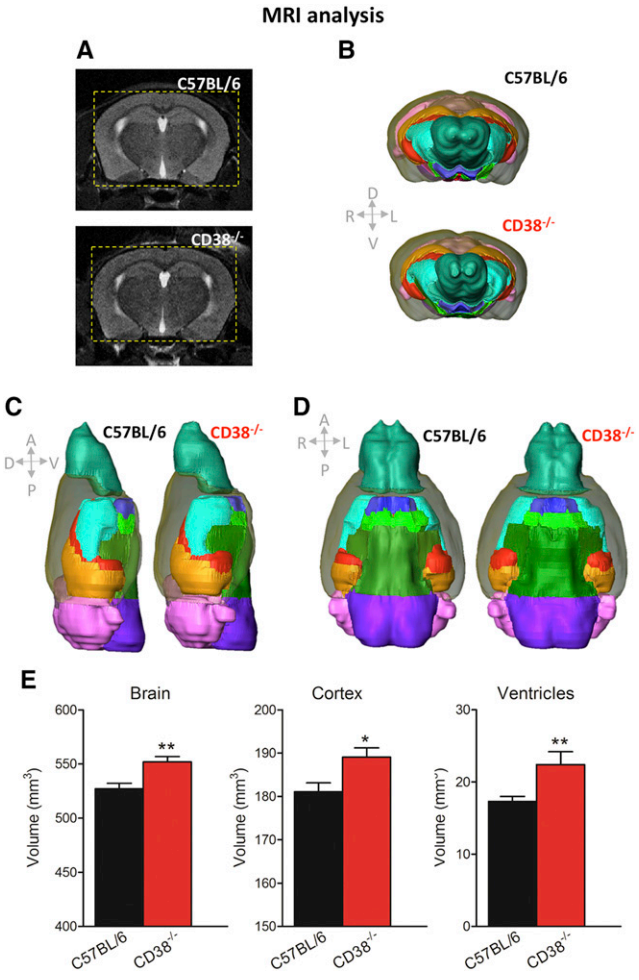

Figure 1. Alteration of brain volumetric integrity in CD38$^{-/-}$ male mice evaluated by MRI. *A*) Sample MRI coronal images (top, C57BL/6 mouse; bottom, CD38$^{-/-}$ mouse), corresponding to 2-dimensional cutting planes. To better highlight the difference between genotypes, dotted yellow squares were drawn on both images to outline the size of the CD38$^{-/-}$ mice brain compared with the C57BL/6 brain size. *B–D*) 3-dimensional reconstructions of mouse brains with brain regions delineated according to mouse brain atlas (left C57BL/6; right CD38$^{-/-}$ mice), showing significant differences in brain gross anatomy between C57BL/6 mice and CD38$^{-/-}$ mice. Brain regions considered in the analysis are represented by distinct colors as follows: ventricles, red; cortex, gray; hippocampi, orange; ventral structures, green; striatum, turquoise; olfactory bulbs, blue-green; cerebellum/colliculus, pink and purple. *E*) Histograms of estimated volumes in cubic millimeters of the total brain, cortex and ventricles (C57BL/6, $n = 9$ mice; CD38$^{-/-}$ mice, $n = 10$ mice). Error bars represent SEM. $^*P < 0.05$, $^{**}P < 0.01$ (Mann-Whitney, 2-tailed test).

22.4 ± 1.8 mm^3 for CD38$^{-/-}$ mice *vs.* 17.3 ± 0.7 mm^3 in controls). In contrast, the volumes of other brain structures such as the hippocampus, cerebellum, and olfactory bulbs did not differ between genotypes (unpublished data). We also examined whether juvenile CD38$^{-/-}$ male mice, juvenile CD38$^{-/-}$ female mice, and adult CD38$^{-/-}$ female mice could also display abnormal brain development. No difference was observed between the different groups compared with their respective C57BL/6 controls (Supplemental Fig. S1).

Enhanced E-I balance in PFC networks

We investigated whether the balance between the excitatory and inhibitory inputs, which directs the pyramidal response, might be impaired in CD38$^{-/-}$ mice, knowing that CD38 is normally expressed in pyramidal neurons (45). The L5PyNs mostly elaborate the output signals of the cortex, realizing the spatiotemporal dendritic integration of excitatory and inhibitory signals transmitted by upstream microcircuits (46). To determine the E-I balance, stable somatic voltage-clamp recordings of L5PyNs subthreshold postsynaptic responses evoked by layer 2–3 electrical stimulation at various holding potentials were obtained in the PFC of CD38$^{-/-}$ and C57BL/6 mice (**Fig. 2*A***). The evoked synaptic conductance was extracted (see Materials and Methods) and decomposed into excitatory and inhibitory conductances (Fig. 2*B*). This allowed us to better evaluate the relative contribution of evoked excitatory and inhibitory inputs reaching the soma of the recorded neurons. Layer 2–3 electrical stimulation typically produced a fast excitatory conductance followed by a long-lasting inhibitory conductance. Integrals of excitatory and inhibitory conductances were expressed as a percentage of the integral of the total conductance to determine the E-I balance (32, 34, 36). Quantification of these somatic conductances showed that the evoked composite signal at the soma was composed of 19.3 ± 1.1% of excitation and 80.7 ± 1.1% of inhibition in the PFC of C57BL/6 mice (Fig. 2*C*). In contrast, the E-I balance in CD38$^{-/-}$ mice was significantly shifted toward enhanced excitation (excitation: 24 ± 1.6%; inhibition: 76 ± 1.6%).

Impaired synaptic plasticity in PFC networks

Synaptic plasticity such as LTP in the brain is essential for learning and memory (47–49), but to keep functional neuronal networks (*i.e.*, to ensure the stability of the E-I balance), the inhibitory plasticity has to adjust to the excitatory plasticity (50, 51). Here we applied an HFS protocol in layer 2–3 of the PFC to induce LTP of both excitatory and inhibitory conductances in L5PyNs (Fig. 2*D*). A control experiment in C57BL/6 mice showed that excitatory and inhibitory conductances were enhanced 45 min after HFS by around 50 and 90%, respectively (Fig. 2*E*). Importantly, we found that the potentiation of excitation was greater in CD38$^{-/-}$ mice than in C57BL/6 mice and became significantly more potentiated 45 min after HFS (CD38$^{-/-}$ mice: 143 ± 26.4%; C57BL/6 mice: 51.4 ± 18.6%), whereas potentiation of inhibition was comparable between genotypes (Fig. 2*E*).

Impaired social interactions

Although in ASD various cerebral structures are affected, it appears that the PFC is particularly important. The medial PFC (mPFC) is crucial for the management of social interactions and social cues and recent MRI studies have shown that the PFC is one of the brain structures associated with autistic social behavior (52). Social behavior was first assessed in a specific social interaction task that

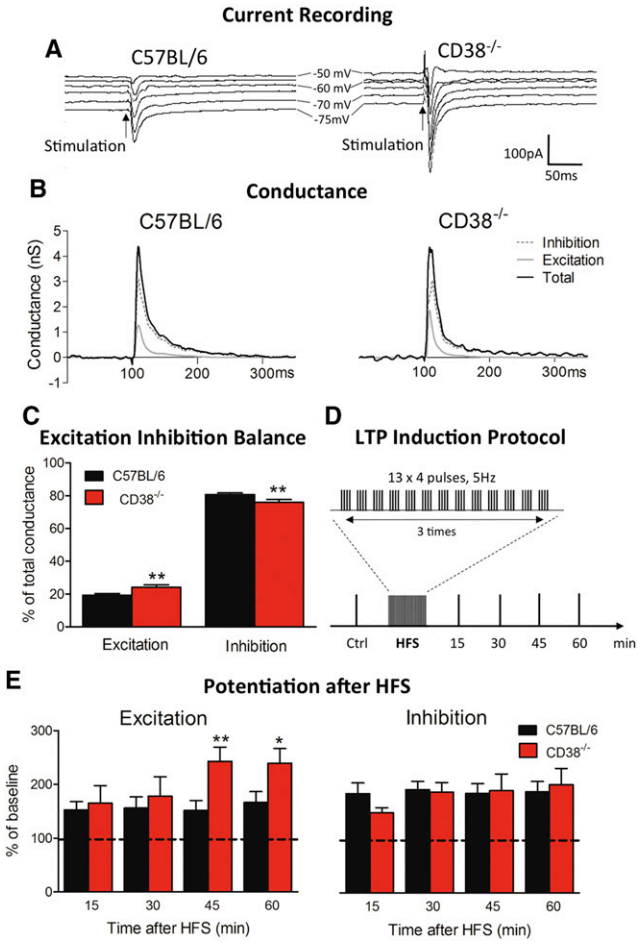

Figure 2. Impaired E-I balance in the PFC of CD38$^{-/-}$ male mice. *A*) Representative current responses in a L5PyN following layer 2-3 stimulation in PFC of a C57BL/6 mouse (left column) and of a CD38$^{-/-}$ mouse (right column), recorded under voltage clamp at various holding potentials (each response is the mean of 5 recordings). Vertical arrows indicate stimulation onset. *B*) Corresponding total conductance changes (black line). Changes in excitatory conductance (light gray line) and inhibitory conductance (dotted dark gray line) derived from total conductance decomposition (see Materials and Methods). *C*) Histograms of the E-I balance. The E-I balance changed significantly in CD38$^{-/-}$ mice (n = 25 cells, 13 mice) compared with C57BL/6 mice (n = 43 cells, 21 mice). $^{**}P < 0.01$ (Mann-Whitney, 2-tailed test). *D*) LTP induction protocol by HFS. *E*) LTP induced in L5PyNs from C57BL/6 mice (n = 11 cells, 8 mice) and CD38$^{-/-}$ mice (n = 8 cells, 5 mice) at 15, 30, 45 and 60 min after the HFS protocol. Histograms represent relative changes compared with control (0 min, before HFS) in integral of excitatory (left panel) and integral of inhibitory (right panel) conductances. Error bars represent SEM. $^{*}P < 0.05$, $^{**}P < 0.01$ (Mann-Whitney, 1-tailed test).

requires integrity of the PFC (53, 54) and in which male mice establish a novel and free interaction when placed together in a novel environment (55, 56). We have previously shown that during the social interaction task, mice exchange acoustic communication signals (39), although this does not occur when mice cannot interact freely (57). In addition, we showed that acoustic communication is correlated to specific social sequences in the social interaction task and can reflect affiliative behaviors, dominance, or aggressiveness (40). Here we showed that the proportion of adult CD38$^{-/-}$ mice vocalizing during this task was significantly lower (20%) than in C57BL/6 mice (64.3%) (**Fig. 3*A***, left panel). As shown in Fig. 3*A* (center panel), CD38$^{-/-}$ mice spent less time in contact with a stranger conspecific male (42.8 ± 8.4 s) as compared with C57BL/6 mice (69 ± 5.9 s). Importantly, CD38$^{-/-}$ mice showed massive aggressiveness compared with C57BL/6 mice, as reflected by an increased number of bites (Fig. 3*A*, right panel: 12.4 ± 5.6 for CD38$^{-/-}$ mice *vs.* 0.9 ± 0.8 for C57BL/6 mice). To test whether theses alterations occurred earlier in the development, we performed a similar experiment in juvenile mice (P28–30). Interestingly, juvenile CD38$^{-/-}$ mice displayed a deficit of vocalization during the social task, even though they exhibited unaltered social behavior at this age (Fig. 3*B*). The proportion of CD38$^{-/-}$ juvenile mice vocalizing during the task was also significantly lower (11.1%) than in C57BL/6 mice (88.9%) (Fig. 3*B*, left panel). This suggests that impairment in vocal communication precedes deterioration of social behavior, particularly the emergence of an aggressive behavior at adulthood.

We also tested adult mice in a 3-chamber social test, as a control to examine social motivation. In this task, mice with normal social motivation show a preference for a stranger mouse over an unknown object (empty cup) when submitted to a choice between these 2 options. As shown in Fig. 3*C*, in this test, CD38$^{-/-}$ and control mice behaved similarly, spending more time interacting with the stranger mouse than with the unknown object, indicating intact interest for social stimuli (contact duration and numbers with a stranger mouse are similar for CD38$^{-/-}$ mice and for C57BL/6 mice).

Enhanced anxiety-like responses

Aggressive behaviors observed in CD38$^{-/-}$ mice during social interactions prompted us to further characterize emotional reactivity and emotional learning in this model. We first evaluated anxiety-related behavioral responses in these mice using 3 different tests typically used to evaluate anxiety levels in mice. In the light–dark box test, mice had the choice to explore a brightly lit anxiogenic compartment or to stay in a more secure dark compartment. As shown in **Fig. 4*A***, CD38$^{-/-}$ mice showed a significant preference for the dark compartment, as reflected by their longer latencies to enter the lit compartment (56.4 ± 20.9 s for C57BL/6 mice and 216 ± 37.2 s for CD38$^{-/-}$ mice) and reduced number of entries in the lit compartment (6.3 ± 0.4 for C57BL/6 mice and 3.3 ± 1.1 for CD38$^{-/-}$ mice), suggesting a higher level of anxiety in CD38$^{-/-}$ mice. In the elevated plus maze, in which anxiety is induced by the void in elevated open arms, the percentage number of entries and time spent in open arms were not significantly different between CD38$^{-/-}$ mice and C57BL/6 mice (Fig. 4*B*). Moreover, the number of protected and unprotected head dips was also comparable between genotypes (unpublished data), indicating unaltered risk assessment behavior. Finally, we also analyzed locomotion and anxiety-related parameters during exploration of an open

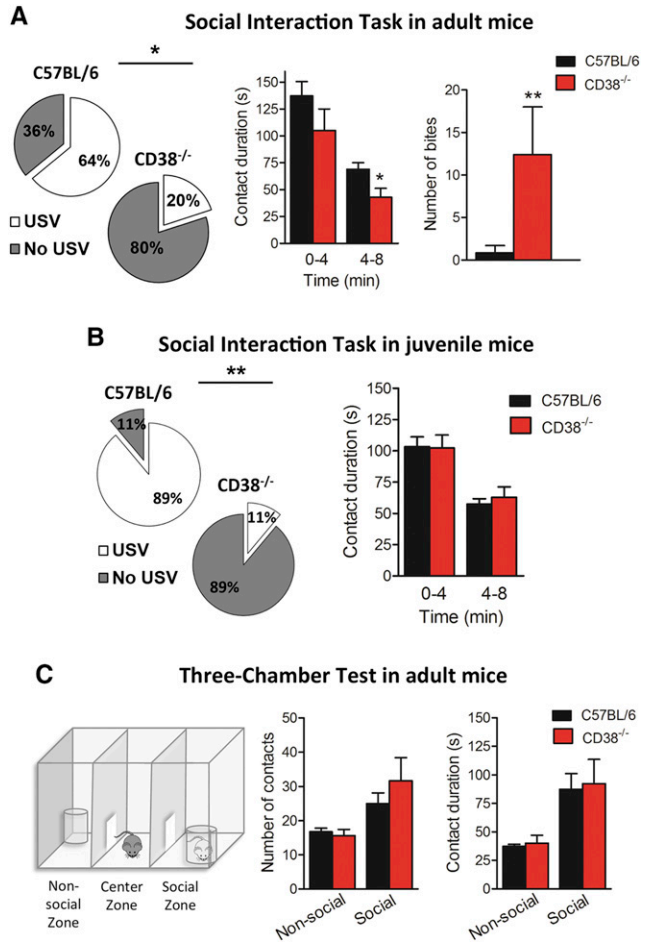

Figure 3. CD38$^{-/-}$ adult male mice display aggressive behavior in a social interaction task. *A*) Left panel shows the analysis of the proportion of mice emitting USVs in the C57BL/6 ($n = 14$ mice) and CD38$^{-/-}$ groups ($n = 10$ mice). White sections represent the proportion of vocalizing mice, and gray sections represent the proportion of nonvocalizing mice. Central histogram shows the time spent in social contact between tested mice (C57BL/6, $n = 14$ mice; CD38$^{-/-}$, $n = 10$ mice) and visitors in an 8-min session. Right histogram shows the number of bites recorded during the session for C57BL/6 mice ($n = 14$) and CD38$^{-/-}$ mice ($n = 10$). *B*) Left panel shows the proportion of juvenile mice emitting USVs (C57BL/6, $n = 9$ mice; CD38$^{-/-}$, $n = 9$ mice). Right histogram shows the time spent in social contact between host juvenile tested mice (C57BL/6, $n = 19$ mice; CD38$^{-/-}$, $n = 13$ mice) and juvenile visitors in a session of 8 min. *C*) Left panel shows an illustration of the 3-chamber test apparatus. The histogram in the center shows the number of social and nonsocial contacts made by C57BL/6 adult mice and CD38$^{-/-}$ adult mice. Right histogram shows contact duration during social and nonsocial contacts in C57BL/6 mice and CD38$^{-/-}$ (C57BL/6, $n = 15$ mice; CD38$^{-/-}$, $n = 10$ mice). Error bars represent SEM. $^{*}P < 0.05$, $^{**}P < 0.01$ (Mann-Whitney, 2-tailed test).

field (Fig. 4C). CD38$^{-/-}$ mice showed a significant reduction in the distance traveled in the open field over the 40-min recording period (46.8 ± 3.6 m for CD38$^{-/-}$ mice and 77.4 ± 5.2 m for C57BL/6), which was associated with a reduced number of entries in the center area (37.9 ± 6.8 for CD38$^{-/-}$ and 74.5 ± 8.8 for C57BL/6), suggesting alterations of both exploration and anxiety-related behavioral responses in CD38$^{-/-}$ mice in this test.

Enhanced emotional reactivity in CD38$^{-/-}$ mice but unaltered fear learning and memory

Emotional learning and memory were first evaluated in a contextual fear-conditioning paradigm, which depends on the integrity of both amygdala and hippocampus (**Fig. 5*A***). In this task, CD38$^{-/-}$ mice consistently showed longer durations of freezing following electric foot shock delivery compared with control mice (Fig. 5*A*, 57.2% at 8 min in CD38$^{-/-}$ mice *vs.* 43.6% in C57BL/6 mice). Mice were placed back in the same context 24, 48, and 72 h after this acquisition session for 20 min each day without any foot shock delivery. Mice of both genotypes showed long freezing responses at the beginning of each session, reflecting strong retention of contextual fear memory, and mice of both genotypes displayed a progressive and parallel decay of freezing behavior during the 20-min sessions, suggesting comparable extinction of the conditioned response in the 2 genotypes. Remarkably, however, the amount of freezing was consistently higher in CD38$^{-/-}$ mice than in control mice throughout the experiment (all sessions), suggesting stronger expression of fear responses rather than genuine differences in learning and memory performances. In an amygdala-dependent auditory-cued fear-conditioning paradigm (Fig. 5*B*), the percentage of freezing was also significantly increased in CD38$^{-/-}$ mice compared with C57BL/6 mice during the first and second tone deliveries during acquisition session (CS1, CS2). Increased freezing during first tone delivery (*i.e.*, before any foot shock delivery) suggests it reflected increased emotional reactivity rather than increased pain sensitivity. However, the amount of freezing was comparable in CD38$^{-/-}$ and control mice during delivery of the last tone of the acquisition session (CS3) as well as during delivery of the 4 conditioned stimuli during the retention session performed 24 h later (CS1–CS4), suggesting comparable fear learning and memory in the 2 genotypes.

We then investigated auditory perception by comparing ABRs in mice of both genotypes (Fig. 5*C*). CD38$^{-/-}$ mice had normal ABR thresholds in response to pure tones of different frequencies, showing a typical V-shape curve with an optimal threshold detected at 8 kHz, as in C57BL/6 mice, suggesting unaltered hearing capability. We further determined the acoustic startle reflex induced by tone intensities ranging from 70 to 120 dB (Fig. 5*D*) and did not detect any significant genotype effect, suggesting normal reflex responses in CD38$^{-/-}$ mice in response to auditory tones. We then investigated the prepulse inhibition of acoustic startle reflex to evaluate auditory gating (Fig. 5*E*). Non-startling prepulse from 3 to 12 dB above 65 dB background noise (68, 71, 74, and 77 dB) induced a relative decrease in the startle amplitude, which was comparable in CD38$^{-/-}$ and C57BL/6 mice. Overall, CD38$^{-/-}$ mice had no impairment in fear learning and memory tasks, and their general enhancement in freezing duration during conditioning could not be attributed to overt alterations in the perception and processing of auditory stimuli.

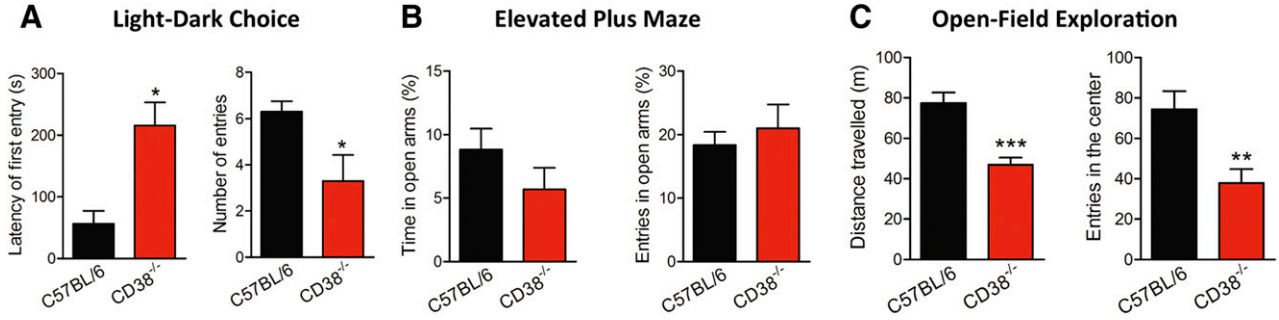

Figure 4. CD38$^{-/-}$ male mice show high levels of anxiety. *A*) Latency of first entry in the lit compartment and number of entries in the lit compartment during the light–dark test. *B*) Behavioral responses in the elevated plus-maze test expressed as the percent time spent and number of entries in the open arms. *C*) Distance traveled and number of entries in the center in the open-field test. C57BL/6, $n = 10$ mice; CD38$^{-/-}$ mice, $n = 10$ mice. Error bars represent SEM. $^{*}P < 0.05$, $^{**}P < 0.01$, $^{***}P < 0.001$ (Mann-Whitney, 2-tailed test).

Neurochemical levels impairment in CD38$^{-/-}$ mice

A seminal study from Higashida's group revealed that CD38$^{-/-}$ mice on an Institute of Cancer Research genetic background display low plasma levels of OT (29). Using a radioimmunoassay, we investigated whether CD38$^{-/-}$ mice under a C57BL/6 genetic background display similar characteristic. We found that adult male CD38$^{-/-}$ mice have lower levels of plasma OT compared with adult C57BL/6 control mice (**Fig. 6*A***, 12.4 ± 1.2 pg/ml for CD38$^{-/-}$ mice *vs.* 98 ± 1.4 pg/ml for C57BL/6 mice). We found similar reductions in OT levels in juvenile CD38$^{-/-}$ male mice, juvenile CD38$^{-/-}$ females, and adult CD38$^{-/-}$ females (Supplemental Fig. S2*A*–*D*). However, OT may not be the sole neuromodulator altered in CD38$^{-/-}$ mice, and it is known that monoamines contribute to flexible behaviors mainly *via* prefrontal modulation. Neurotransmitters such as NE, 5-HT, and DA have been shown to be associated with aggressive- and anxiety-related behaviors. However, there is currently no information on the levels of any monoamine and their metabolites in CD38$^{-/-}$ mice. We used ultra-performance liquid chromatography to measure the content of endogenous monoamines and their respective metabolites in frozen PFC samples. We found that the basal levels of NE (Fig. 6*B*, +35%) as well as that of 5-HT (+151%), and its metabolite 5-hydroxyindoleacetic acid (5-HIAA) (Fig. 6*C*, +136%) were significantly increased in CD38$^{-/-}$ mice compared with C57BL/6 mice in the PFC. Finally, we found that the basal level of DA was unchanged in CD38$^{-/-}$, whereas 3,4-dihydroxyphenylacetic acid (DOPAC) (+453%) and homovanillic acid (HVA) (+124%), 2 main metabolites of DA, were found to have significantly increased in CD38$^{-/-}$ mice (Fig. 6*D*), suggesting a higher DA turnover in CD38$^{-/-}$ mice compared with control mice. We also measured monoamine levels in juvenile CD38$^{-/-}$ male, juvenile CD38$^{-/-}$ female, and adult CD38$^{-/-}$ female mice. We found very modest changes in levels of 5-HT and 5-HIAA in adult female and juvenile female, respectively (Supplemental Fig. S2*F*, *H*). In the case of the juvenile CD38$^{-/-}$ male mice, only a very modest reduction in NE was observed (Supplemental Fig. S2*G*).

DISCUSSION

Here we report that CD38$^{-/-}$ male mice show an abnormal development of the cortex and we also provide the first direct evidence that this is associated with an E-I balance shifted toward higher excitation and altered synaptic plasticity in the PFC. Importantly, we also show that the PFC of these mice show alterations in monoamine levels involved in the control of flexible behaviors. At the behavioral level we demonstrate that a social interaction task relying on the PFC is compromised in CD38$^{-/-}$ mice. Acoustic communication is markedly altered in these mice, and we show that this impairment precedes development of enhanced aggressiveness in adult CD38$^{-/-}$ mice. Moreover, our data indicate that the behavioral disturbances displayed by CD38$^{-/-}$ mice cannot be attributed to changes in the perception or gating of auditory stimuli but are associated with higher levels of emotional reactivity in anxiety tests and fear-conditioning tasks. Overall, our data bring new evidences that the CD38$^{-/-}$ mouse could be a relevant model to study pathophysiological brain mechanisms associated with ASD.

Previous studies in CD38$^{-/-}$ mice suggested that CD38 plays a critical role in social behavior by regulating the secretion of OT by hypothalamus, and the deficits in these mice were also associated with observation of a decrease in maternal care and impaired social memory (29). These profound behavioral abnormalities make CD38$^{-/-}$ mice an important model candidate in the study of neurodevelopmental pathologies such as ASD. Indeed, numerous studies pointed toward a deficit in OT signaling in patients with ASD (18), and a common SNP has been associated with a familial form of autism (*CD38* rs3796863). Additionally, individuals with the CD38 "risk allele" (CC) have lower expression of CD38 and lower plasma levels of OT. ASD patients with this CC risk allele are more severely affected than ASD patients with the AA allele (19, 21). However, OT deficit is currently not considered as the primary cause of ASD but has rather been suggested to worsen the social deficits.

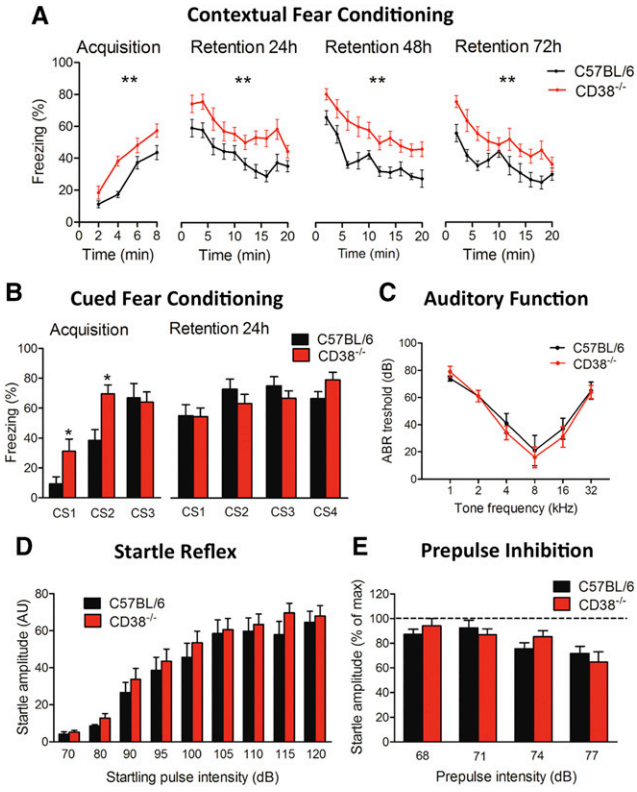

Figure 5. Enhanced emotional reactivity in CD38$^{-/-}$ male mice. *A*) Contextual fear conditioning. The plot shows the percent freezing recorded in C57BL/6 (n = 10 mice) and CD38$^{-/-}$ mice (n = 10 mice) during the acquisition session (8 min, 4 shocks delivered) and during successive retention sessions (24, 48, and 72 h). $^{**}P < 0.01$ (2-way ANOVA). *B*) Auditory-cued fear conditioning (C57BL/6, n = 9; CD38$^{-/-}$ mice, n = 10). Percent freezing was calculated during presentation of the CS (tone lasting 30 s) during acquisition (CS1–3 each followed by 1 foot shock or UCS and during retention (CS1–4 not followed by UCS). $^{*}P < 0.05$ (Mann-Whitney, 2-tailed test). *C*) ABR recorded in C57BL/6 (n = 5 mice) and CD38$^{-/-}$ mice (n = 5 mice). ABR thresholds are presented as a function of pure tone frequencies. Statistical analysis using a 2-way ANOVA. *D*) Acoustic startle reflex of C57BL/6 mice (n = 9 mice) and CD38$^{-/-}$ mice (n = 10 mice). The acoustic startle reflex response increased when raising startling pulse intensities from 70 to 120 dB. Statistical analysis using Mann-Whitney, 2-tailed test. *E*) Prepulse inhibition of the acoustic startle reflex expressed as the amplitude of the startle response when a prepulse of 3, 6, 9, or 12 dB above background noise (65 dB) preceded the startling pulse. Data are normalized to the maximal amplitude recorded in the absence of prepulse (C57BL/6, n = 9 mice; CD38$^{-/-}$, n = 10 mice). Mann-Whitney, 2-tailed test. Error bars represent SEM.

Excessive cerebral growth during development has been reported in ASD patients, especially at the PFC level. Many studies have found an abnormally high number of neurons in the human cortex (2, 58). Here, our *in vivo* MRI volumetric measurements clearly show a selective increase of cortical size in adult CD38$^{-/-}$ male mice not seen in adult female mice or juvenile mice. The mechanism of this gender-specific abnormal brain growth is not clear. However, this phenomenon is not restricted to the brain because it has also been reported that CD38$^{-/-}$ male mice show cardiac hypertrophy, whereas female CD38$^{-/-}$ mice display normal heart development (59). In adult CD38$^{-/-}$ male mice, the simplest explanation would be that CD38 deletion has altered early adult brain modifications such as either an ongoing brain growth occurring in early adulthood or due to a reduced activity of pruning or neuronal apoptosis during this later period. Consistent with this hypothesis, CD38 is expressed at the embryonic stage (60, 61) and its expression is known to be involved in neural differentiation and microglia activation (62–64). Therefore, deleting CD38 may have promoted cell proliferation (62, 65) leading to excessive growth of cortical layers.

The cerebral cortex consists mainly of pyramidal excitatory glutamatergic neurons (about 80%) and inhibitory GABAergic interneurons (about 20%) (66). Intriguingly, the cerebral structures involved in ASD seem to be diverse, but among them the PFC holds an important place. The mPFC plays a critical role in the treatment of information during social interactions (53, 67, 68), and recent functional MRI studies have shown that the mPFC is one of the brain structures associated with altered social behavior in ASD patients (52). CD38 is involved in a variety of cellular processes because it is widely expressed in pyramidal neurons (45), astrocytes (69), and microglia (64). One main goal of our study was to explore whether and how CD38 loss of function may impact the physiologic control of neural networks in the PFC. The E-I balance determined at the level of the L5PyNs of C57BL/6 mice was around 19–81%, which is not different from the balance determined in mPFC of another control mouse line [*e.g.*, 129/SV line: 20–80% (70)] or in other cortical structures such as the rat visual cortex [20–80% (32)]. These E-I balance values are within a narrow range, consistent with the existence of a specific set-point required to maintain a coherent functioning of neural networks (50, 71). The increased E-I balance in CD38$^{-/-}$ mice may result from an increase in the number or weight of glutamatergic synapses and a decrease in the number or weight of GABAergic synapses. This hypothesis is consistent with the involvement of CD38 in a neurodevelopmental disease such as ASD, in which significant neuronal network remodeling has been observed (72, 73). The CD38 signaling pathway is recruited by several GPCRs, which could normally participate in the establishment of neural networks within the mPFC and thereby directly or indirectly modulate the E-I balance. Interestingly, the PFC is one of the structures that have been reported to be rich in OT receptors (74); therefore, a reduction in OT signaling might affect the E-I balance. Supporting this view, recent articles have outlined the important role of OT in synapse maturation and in synaptic transmission and plasticity (14–17). However, OT is not the sole neuromodulator altered in CD38$^{-/-}$ mice because we also report here an increased turnover of 5-HT and DA in the PFC of adult CD38$^{-/-}$ male mice. These biochemical changes also have to be considered knowing that in our previous studies we have shown that the fine-tuning of the E-I balance is linked to the action of numerous neuromodulators such as DA and 5-HT (37, 70).

Genetic models of autism, such as *Shank3*$^{-/-}$ and *Nlgn3*$^{-/-}$ mice, and the pharmacological (valproic acid) mouse model, are often associated with changes in long-term

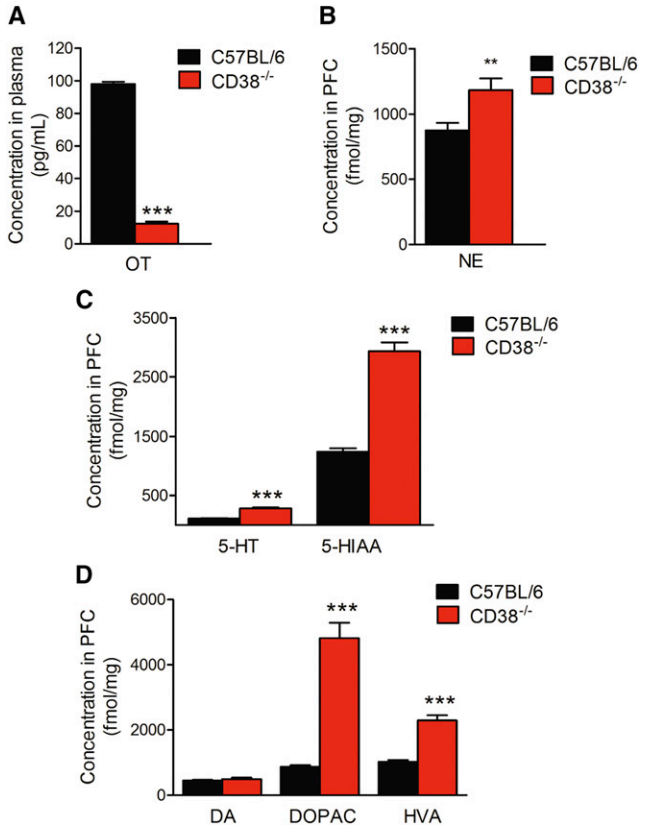

Figure 6. Alteration of endogenous neurochemical levels in CD38$^{-/-}$ male mice. *A*) Plasma levels of OT. *B*) PFC endogenous content of NE in C57BL/6 mice and CD38$^{-/-}$ mice. *C*) PFC endogenous content of 5-HT and 5-HIAA in C57BL/6 and CD38$^{-/-}$ mice. *D*) PFC endogenous content of DA, DOPAC, and HVA in C57BL/6 and CD38$^{-/-}$ mice. C57BL/6 mice, $n = 10$ mice; CD38$^{-/-}$ mice, $n = 10$ mice. Error bars represent SEM. $^{**}P < 0.01$, $^{***}P < 0.001$ (Mann-Whitney, 2-tailed test).

plasticity and NMDA currents. Here, we found that LTP is increased in the mPFC of CD38$^{-/-}$ mice, which is the first report of altered cortical plasticity in this model. In CD38$^{-/-}$ mice, the excitatory component was excessively potentiated, whereas the potentiation of the inhibitory component was similar to that recorded in mPFC of control mice. This suggests that deletion of CD38 led to an increase of neuronal excitability and facilitated potentiation of AMPAR (α-amino-3-hydroxy-5-methyl-4-isoxazolepropionic acid receptor)–dependent currents.

At the behavioral level, adult male CD38$^{-/-}$ mice displayed a deficit in social interaction and reduced emission of USV along with enhanced aggressiveness. Social interactions involve a circuit of brain structures that includes PFC, hippocampus, amygdala, or other cortical areas susceptible to be altered in ASD. The E-I balance of the PFC is important for both normal and pathologic social interactions (75, 76), and we demonstrate here that both social interactions and the E-I balance of the PFC are dysfunctional in the absence of CD38. Our results in juvenile male mice indicate that a decrease in USV emission rate (77) preceded the social alterations seen in adults. It is thus plausible that an early decrease in communication abilities favored emergence of nonadapted social behavior and aggressiveness in adulthood that might be linked to OT deficits (78). This relationship between OT levels and social behavior would remain to be fully investigated in CD38$^{-/-}$ female mice. In line with this hypothesis, our previous study comparing distinct mouse strains highlighted that aggressiveness is markedly promoted by low capability to vocalize during social interaction (40). The enhanced anxiety-like responses observed here in CD38$^{-/-}$ mice could also contribute to alteration of social behavior. This view is largely supported by the strong comorbidity of anxiety disorders with social cognitive disorders and by the involvement of an integrated brain circuit including amygdala, hypothalamus, and PFC in the control of innate social behaviors such as aggression and parenting responses [(79) for a review]. Previous studies in CD38$^{-/-}$ mice reported variable effects of CD38 loss of function on anxiety and parenting behaviors (29, 80). In the present study, CD38$^{-/-}$ mice displayed enhanced anxiety-like responses during open-field and light–dark choice testing but not in the elevated plus-maze anxiety test. This variability may depend on the genetic background or on the specific pattern of neurotransmitter and OT signaling alterations (78, 81). This latter hypothesis may be particularly relevant in CD38$^{-/-}$ mice in which we detected increased levels of NE and 5-HT, which has been shown to be formerly associated with increased aggressiveness (54, 82) and impaired social and nonsocial decision-making processes (54, 83), respectively. We have evidence that appropriates integration of social cues and adequate response to an unknown social conspecific rely on the integrity of the PFC (53). The impaired ability of CD38$^{-/-}$ mice to integrate social cues, such as the vocal ones, may have favored aggressive reactions, despite unaltered propensity to seek social contact. As suggested in earlier studies (84), it is also likely that PFC-dependent executive dysfunctions more importantly affected CD38$^{-/-}$ mice behavior during direct social interactions, in which it is required to rapidly adapt to the encounter's behavioral responses, than during simple approach responses in the 3-chamber test, which may involve lower PFC demand. The high levels of OT receptors in PFC (74) suggest that a neuronal OT signaling defect may also contribute to their aggressive behavior, as reported in OT-null mutant mice (78).

In summary, our results show that the CD38$^{-/-}$ mice are characterized by a modification of the E-I balance that could be explained by an alteration in the development of PFC neural networks. In another animal model ($\beta_2^{-/-}$ mice) also exhibiting marked social disorganization, we previously showed the E-I balance alteration to be associated with an impaired decision-making process (85). We confirm here that compromising the E-I balance of the PFC may be associated with extensive social defects. The presence of OT signaling impairment in CD38$^{-/-}$ mice and its association with critical behavioral monoamine deregulations and neurobiological alterations bring strong support to consider CD38$^{-/-}$ mice as a mouse model for studying ASD. Whether the panel of behavioral deficits exhibited by CD38$^{-/-}$ animals are interrelated is currently unknown, but we have paved the way here for novel avenues that could be investigated with the help of this model. In particular, this study suggests that future therapies for ASD

patients with the common SNP (*CD38* rs3796863) should also consider how OT and monoamines signaling interact and control neuronal network activity. FJ

ACKNOWLEDGMENTS

The authors thank Dr. Frances Lund (University of Alabama–Birmingham, Birmingham, AL, USA) for providing $CD38^{-/-}$ mice. This research was supported by grants from Centre National de la Recherche Scientifique (CNRS), INSERM, Paris-Sud University. Funding for this work was provided by la Fondation Jérôme Lejeune (to J.-M.C. and P.F.), and by an international CNRS Laboratoire international Associé(LIA) grant (to J.-M.C. and A.G.). L.L.M. and A.Z. are recipients of a Ph.D. fellowship from Paris-Sud University. The authors also thank the zootechnic platform at the Neuroscience Paris-Saclay Institute for mice breeding and care. This work was also partly funded by France Life Imaging Grant ANR-11-INBS-0006. The authors declare no conflicts of interest.

AUTHOR CONTRIBUTIONS

A. Galione, S. de la Porte, P. Fossier, S. Granon, C. Vaillend, and J.-M. Cancela conceived and designed the experiments; L. L. Martucci, M. Amar, R. Chaussenot, G. Benet, O. Bauer, J. Callebert, C. Sebrié, J.-M. Edeline, and J.-M. Launay performed experiments; L. L. Martucci, M. Amar, R. Chaussenot, G. Benet, O. Bauer, A. de Zélocourt, A. Nosjean, J.-M. Launay, J. Callebert, C. Sebrié, J.-M. Edeline, S. de la Porte, P. Fossier, S. Granon, C. Vaillend, and J.-M. Cancela analyzed data; and L. L. Martucci, A. Galione, S. de la Porte, P. Fossier, S. Granon, C. Vaillend, and J.-M. Cancela wrote the manuscript.

REFERENCES

1. Bourgeron, T. (2016) Current knowledge on the genetics of autism and propositions for future research. *C. R. Biol.* **339**, 300–307
2. Courchesne, E., Mouton, P. R., Calhoun, M. E., Semendeferi, K., Ahrens-Barbeau, C., Hallet, M. J., Barnes, C. C., and Pierce, K. (2011) Neuron number and size in prefrontal cortex of children with autism. *JAMA* **306**, 2001–2010
3. Jamain, S., Quach, H., Betancur, C., Råstam, M., Colineaux, C., Gillberg, I. C., Soderstrom, H., Giros, B., Leboyer, M., Gillberg, C., and Bourgeron, T.; Paris Autism Research International Sibpair Study. (2003) Mutations of the X-linked genes encoding neuroligins NLGN3 and NLGN4 are associated with autism. *Nat. Genet.* **34**, 27–29
4. Durand, C. M., Betancur, C., Boeckers, T. M., Bockmann, J., Chaste, P., Fauchereau, F., Nygren, G., Rastam, M., Gillberg, I. C., Anckarsäter, H., Sponheim, E., Goubran-Botros, H., Delorme, R., Chabane, N., Mouren-Simeoni, M.-C., de Mas, P., Bieth, E., Rogé, B., Héron, D., Burglen, L., Gillberg, C., Leboyer, M., and Bourgeron, T. (2007) Mutations in the gene encoding the synaptic scaffolding protein SHANK3 are associated with autism spectrum disorders. *Nat. Genet.* **39**, 25–27
5. Peça, J., Feliciano, C., Ting, J. T., Wang, W., Wells, M. F., Venkatraman, T. N., Lascola, C. D., Fu, Z., and Feng, G. (2011) Shank3 mutant mice display autistic-like behaviours and striatal dysfunction. *Nature* **472**, 437–442
6. Harony-Nicolas, H., Kay, M., Hoffmann, J. D., Klein, M. E., Bozdagi-Gunal, O., Riad, M., Daskalakis, N. P., Sonar, S., Castillo, P. E., Hof, P. R., Shapiro, M. L., Baxter, M. G., Wagner, S., and Buxbaum, J. D. (2017) Oxytocin improves behavioral and electrophysiological deficits in a novel Shank3-deficient rat. *eLife* **6**, e18904
7. Chanda, S., Aoto, J., Lee, S.-J., Wernig, M., and Südhof, T. C. (2016) Pathogenic mechanism of an autism-associated neuroligin mutation involves altered AMPA-receptor trafficking. *Mol. Psychiatry* **21**, 169–177
8. Auerbach, B. D., Osterweil, E. K., and Bear, M. F. (2011) Mutations causing syndromic autism define an axis of synaptic pathophysiology. *Nature* **480**, 63–68
9. Bourgeron, T. (2015) From the genetic architecture to synaptic plasticity in autism spectrum disorder. *Nat. Rev. Neurosci.* **16**, 551–563
10. Rubenstein, J. L. R., and Merzenich, M. M. (2003) Model of autism: increased ratio of excitation/inhibition in key neural systems. *Genes Brain Behav.* **2**, 255–267
11. Yizhar, O., Fenno, L. E., Prigge, M., Schneider, F., Davidson, T. J., O'Shea, D. J., Sohal, V. S., Goshen, I., Finkelstein, J., Paz, J. T., Stehfest, K., Fudim, R., Ramakrishnan, C., Huguenard, J. R., Hegemann, P., and Deisseroth, K. (2011) Neocortical excitation/inhibition balance in information processing and social dysfunction. *Nature* **477**, 171–178
12. Nelson, S. B., and Valakh, V. (2015) Excitatory/inhibitory balance and circuit homeostasis in autism spectrum disorders. *Neuron* **87**, 684–698
13. Powell, K. (2004) Opening a window to the autistic brain. *PLoS Biol.* **2**, E267
14. Tyzio, R., Nardou, R., Ferrari, D. C., Tsintsadze, T., Shahrokhi, A., Eftekhari, S., Khalilov, I., Tsintsadze, V., Brouchoud, C., Chazal, G., Lemonnier, E., Lozovaya, N., Burnashev, N., and Ben-Ari, Y. (2014) Oxytocin-mediated GABA inhibition during delivery attenuates autism pathogenesis in rodent offspring. *Science* **343**, 675–679
15. Marlin, B. J., Mitre, M., D'amour, J. A., Chao, M. V., and Froemke, R. C. (2015) Oxytocin enables maternal behaviour by balancing cortical inhibition. *Nature* **520**, 499–504
16. Owen, S. F., Tuncdemir, S. N., Bader, P. L., Tirko, N. N., Fishell, G., and Tsien, R. W. (2013) Oxytocin enhances hippocampal spike transmission by modulating fast-spiking interneurons. *Nature* **500**, 458–462
17. Zheng, J.-J., Li, S.-J., Zhang, X.-D., Miao, W.-Y., Zhang, D., Yao, H., and Yu, X. (2014) Oxytocin mediates early experience-dependent cross-modal plasticity in the sensory cortices. *Nat. Neurosci.* **17**, 391–399
18. Andari, E., Duhamel, J.-R., Zalla, T., Herbrecht, E., Leboyer, M., and Sirigu, A. (2010) Promoting social behavior with oxytocin in high-functioning autism spectrum disorders. *Proc. Natl. Acad. Sci. USA* **107**, 4389–4394
19. Lerer, E., Levi, S., Israel, S., Yaari, M., Nemanov, L., Mankuta, D., Nurit, Y., and Ebstein, R. P. (2010) Low CD38 expression in lymphoblastoid cells and haplotypes are both associated with autism in a family-based study. *Autism Res.* **3**, 293–302
20. Modahl, C., Green, L., Fein, D., Morris, M., Waterhouse, L., Feinstein, C., and Levin, H. (1998) Plasma oxytocin levels in autistic children. *Biol. Psychiatry* **43**, 270–277
21. Munesue, T., Yokoyama, S., Nakamura, K., Anitha, A., Yamada, K., Hayashi, K., Asaka, T., Liu, H.-X., Jin, D., Koizumi, K., Islam, M. S., Huang, J.-J., Ma, W.-J., Kim, U.-H., Kim, S.-J., Park, K., Kim, D., Kikuchi, M., Ono, Y., Nakatani, H., Suda, S., Miyachi, T., Hirai, H., Salmina, A., Pichugina, Y. A., Soumarokov, A. A., Takei, N., Mori, N., Tsujii, M., Sugiyama, T., Yagi, K., Yamagishi, M., Sasaki, T., Yamasue, H., Kato, N., Hashimoto, R., Taniike, M., Hayashi, Y., Hamada, J., Suzuki, S., Ooi, A., Noda, M., Kamiyama, Y., Kido, M. A., Lopatina, O., Hashii, M., Amina, S., Malavasi, F., Huang, E. J., Zhang, J., Shimizu, N., Yoshikawa, T., Matsushima, A., Minabe, Y., and Higashida, H. (2010) Two genetic variants of CD38 in subjects with autism spectrum disorder and controls. *Neurosci. Res.* **67**, 181–191
22. Zhang, H.-F., Dai, Y.-C., Wu, J., Jia, M.-X., Zhang, J.-S., Shou, X.-J., Han, S.-P., Zhang, R., and Han, J.-S. (2016) Plasma oxytocin and arginine-vasopressin levels in children with autism spectrum disorder in China: associations with symptoms. *Neurosci. Bull.* **32**, 423–432
23. Feldman, R., Zagoory-Sharon, O., Weisman, O., Schneiderman, I., Gordon, I., Maoz, R., Shalev, I., and Ebstein, R. P. (2012) Sensitive parenting is associated with plasma oxytocin and polymorphisms in the OXTR and CD38 genes. *Biol. Psychiatry* **72**, 175–181
24. Parker, K. J., Oztan, O., Libove, R. A., Sumiyoshi, R. D., Jackson, L. P., Karhson, D. S., Summers, J. E., Hinman, K. E., Motonaga, K. S., Phillips, J. M., Carson, D. S., Garner, J. P., and Hardan, A. Y. (2017) Intranasal oxytocin treatment for social deficits and biomarkers of response in children with autism. *Proc. Natl. Acad. Sci. USA* **114**, 8119–8124
25. Cancela, J. M., Churchill, G. C., and Galione, A. (1999) Coordination of agonist-induced Ca2+-signalling patterns by NAADP in pancreatic acinar cells. *Nature* **398**, 74–76
26. Lee, H. C. (2001) Physiological functions of cyclic ADP-ribose and NAADP as calcium messengers. *Annu. Rev. Pharmacol. Toxicol.* **41**, 317–345

27. Cosker, F., Cheviron, N., Yamasaki, M., Menteyne, A., Lund, F. E., Moutin, M.-J., Galione, A., and Cancela, J.-M. (2010) The ecto-enzyme CD38 is a nicotinic acid adenine dinucleotide phosphate (NAADP) synthase that couples receptor activation to Ca2+ mobilization from lysosomes in pancreatic acinar cells. *J. Biol. Chem.* **285**, 38251–38259
28. Chini, C. C. S., Tarragó, M. G., and Chini, E. N. (2017) NAD and the aging process: role in life, death and everything in between. *Mol. Cell. Endocrinol.* **455**, 62–74
29. Jin, D., Liu, H.-X., Hirai, H., Torashima, T., Nagai, T., Lopatina, O., Shnayder, N. A., Yamada, K., Noda, M., Seike, T., Fujita, K., Takasawa, S., Yokoyama, S., Koizumi, K., Shiraishi, Y., Tanaka, S., Hashii, M., Yoshihara, T., Higashida, K., Islam, M. S., Yamada, N., Hayashi, K., Noguchi, N., Kato, I., Okamoto, H., Matsushima, A., Salmina, A., Munesue, T., Shimizu, N., Mochida, S., Asano, M., and Higashida, H. (2007) CD38 is critical for social behaviour by regulating oxytocin secretion. *Nature* **446**, 41–45
30. Higashida, H. (2016) Somato-axodendritic release of oxytocin into the brain due to calcium amplification is essential for social memory. *J. Physiol. Sci.* **66**, 275–282
31. Partida-Sánchez, S., Cockayne, D. A., Monard, S., Jacobson, E. L., Oppenheimer, N., Garvy, B., Kusser, K., Goodrich, S., Howard, M., Harmsen, A., Randall, T. D., and Lund, F. E. (2001) Cyclic ADP-ribose production by CD38 regulates intracellular calcium release, extracellular calcium influx and chemotaxis in neutrophils and is required for bacterial clearance in vivo. *Nat. Med.* **7**, 1209–1216
32. Le Roux, N., Amar, M., Baux, G., and Fossier, P. (2006) Homeostatic control of the excitation-inhibition balance in cortical layer 5 pyramidal neurons. *Eur. J. Neurosci.* **24**, 3507–3518
33. Lucas-Meunier, E., Monier, C., Amar, M., Baux, G., Frégnac, Y., and Fossier, P. (2009) Involvement of nicotinic and muscarinic receptors in the endogenous cholinergic modulation of the balance between excitation and inhibition in the young rat visual cortex. *Cereb. Cortex* **19**, 2411–2427
34. Moreau, A. W., Amar, M., Le Roux, N., Morel, N., and Fossier, P. (2010) Serotoninergic fine-tuning of the excitation-inhibition balance in rat visual cortical networks. *Cereb. Cortex* **20**, 456–467
35. Moreau, A. W., Amar, M., Callebert, J., and Fossier, P. (2013) Serotonergic modulation of LTP at excitatory and inhibitory synapses in the developing rat visual cortex. *Neuroscience* **238**, 148–158
36. Meunier, C. N. J., Amar, M., Lanfumey, L., Hamon, M., and Fossier, P. (2013) 5-HT(1A) receptors direct the orientation of plasticity in layer 5 pyramidal neurons of the mouse prefrontal cortex. *Neuropharmacology* **71**, 37–45
37. Meunier, C. N. J., Cancela, J.-M., and Fossier, P. (2017) Lack of GSK3β activation and modulation of synaptic plasticity by dopamine in 5-HT1A-receptor KO mice. *Neuropharmacology* **113**, 124–136
38. Granon, S., Faure, P., and Changeux, J.-P. (2003) Executive and social behaviors under nicotinic receptor regulation. *Proc. Natl. Acad. Sci. USA* **100**, 9596–9601
39. Chabout, J., Serreau, P., Ey, E., Bellier, L., Aubin, T., Bourgeron, T., and Granon, S. (2012) Adult male mice emit context-specific ultrasonic vocalizations that are modulated by prior isolation or group rearing environment. *PLoS One* **7**, e29401
40. Faure, A., Pittaras, E., Nosjean, A., Chabout, J., Cressant, A., and Granon, S. (2017) Social behaviors and acoustic vocalizations in different strains of mice. *Behav. Brain Res.* **320**, 383–390
41. Willott, J. F., and Erway, L. C. (1998) Genetics of age-related hearing loss in mice. IV. Cochlear pathology and hearing loss in 25 BXD recombinant inbred mouse strains. *Hear. Res.* **119**, 27–36
42. Willott, J. F. (2006) Measurement of the auditory brainstem response (ABR) to study auditory sensitivity in mice. *Curr. Protoc. Neurosci.* **Chapter 8**, Unit8.21B.
43. Landgraf, R., and Neumann, I. D. (2004) Vasopressin and oxytocin release within the brain: a dynamic concept of multiple and variable modes of neuropeptide communication. *Front. Neuroendocrinol.* **25**, 150–176
44. Neumann, I. D., Maloumby, R., Beiderbeck, D. I., Lukas, M., and Landgraf, R. (2013) Increased brain and plasma oxytocin after nasal and peripheral administration in rats and mice. *Psychoneuroendocrinology* **38**, 1985–1993
45. Yamada, M., Mizuguchi, M., Otsuka, N., Ikeda, K., and Takahashi, H. (1997) Ultrastructural localization of CD38 immunoreactivity in rat brain. *Brain Res.* **756**, 52–60
46. Binzegger, T., Douglas, R. J., and Martin, K. A. C. (2004) A quantitative map of the circuit of cat primary visual cortex. *J. Neurosci.* **24**, 8441–8453
47. Bliss, T. V., and Lomo, T. (1973) Long-lasting potentiation of synaptic transmission in the dentate area of the anaesthetized rabbit following stimulation of the perforant path. *J. Physiol.* **232**, 331–356
48. Malenka, R. C., and Nicoll, R. A. (1999) Long-term potentiation–a decade of progress? *Science* **285**, 1870–1874
49. Kemp, A., and Manahan-Vaughan, D. (2004) Hippocampal long-term depression and long-term potentiation encode different aspects of novelty acquisition. *Proc. Natl. Acad. Sci. USA* **101**, 8192–8197
50. Le Roux, N., Amar, M., Moreau, A., Baux, G., and Fossier, P. (2008) Impaired GABAergic transmission disrupts normal homeostatic plasticity in rat cortical networks. *Eur. J. Neurosci.* **27**, 3244–3256
51. Castillo, P. E., Chiu, C. Q., and Carroll, R. C. (2011) Long-term plasticity at inhibitory synapses. *Curr. Opin. Neurobiol.* **21**, 328–338
52. Watanabe, T., Yahata, N., Abe, O., Kuwabara, H., Inoue, H., Takano, Y., Iwashiro, N., Natsubori, T., Aoki, Y., Takao, H., Sasaki, H., Gonoi, W., Murakami, M., Katsura, M., Kunimatsu, A., Kawakubo, Y., Matsuzaki, H., Tsuchiya, K. J., Kato, N., Kano, Y., Miyashita, Y., Kasai, K., and Yamasue, H. (2012) Diminished medial prefrontal activity behind autistic social judgments of incongruent information. *PLoS One* **7**, e39561
53. Avale, M. E., Chabout, J., Pons, S., Serreau, P., De Chaumont, F., Olivo-Marin, J.-C., Bourgeois, J.-P., Maskos, U., Changeux, J.-P., and Granon, S. (2011) Prefrontal nicotinic receptors control novel social interaction between mice. *FASEB J.* **25**, 2145–2155
54. Coura, R. S., Cressant, A., Xia, J., de Chaumont, F., Olivo-Marin, J. C., Pelloux, Y., Dalley, J. W., and Granon, S. (2013) Nonaggressive and adapted social cognition is controlled by the interplay between noradrenergic and nicotinic receptor mechanisms in the prefrontal cortex. *FASEB J.* **27**, 4343–4354
55. De Chaumont, F., Coura, R. D.-S., Serreau, P., Cressant, A., Chabout, J., Granon, S., and Olivo-Marin, J.-C. (2012) Computerized video analysis of social interactions in mice. *Nat. Methods* **9**, 410–417
56. Nosjean, A., Cressant, A., de Chaumont, F., Olivo-Marin, J.-C., Chauveau, F., and Granon, S. (2015) Acute stress in adulthood impoverishes social choices and triggers aggressiveness in preclinical models. *Front. Behav. Neurosci.* **8**, 447
57. Chabout, J., Cressant, A., Hu, X., Edeline, J.-M., and Granon, S. (2013) Making choice between competing rewards in uncertain vs. safe social environment: role of neuronal nicotinic receptors of acetylcholine. *Front. Hum. Neurosci.* **7**, 468
58. Khundrakpam, B. S., Lewis, J. D., Kostopoulos, P., Carbonell, F., and Evans, A. C. (2017) Cortical thickness abnormalities in autism spectrum disorders through late childhood, adolescence, and adulthood: a large-scale MRI study. *Cereb. Cortex* **27**, 1721–1731
59. Takahashi, J., Kagaya, Y., Kato, I., Ohta, J., Isoyama, S., Miura, M., Sugai, Y., Hirose, M., Wakayama, Y., Ninomiya, M., Watanabe, J., Takasawa, S., Okamoto, H., and Shirato, K. (2003) Deficit of CD38/cyclic ADP-ribose is differentially compensated in hearts by gender. *Biochem. Biophys. Res. Commun.* **312**, 434–440
60. Ceni, C., Pochon, N., Brun, V., Muller-Steffner, H., Andrieux, A., Grunwald, D., Schuber, F., De Waard, M., Lund, F., Villaz, M., and Moutin, M.-J. (2003) CD38-dependent ADP-ribosyl cyclase activity in developing and adult mouse brain. *Biochem. J.* **370**, 175–183
61. Ceni, C., Pochon, N., Villaz, M., Muller-Steffner, H., Schuber, F., Baratier, J., De Waard, M., Ronjat, M., and Moutin, M.-J. (2006) The CD38-independent ADP-ribosyl cyclase from mouse brain synaptosomes: a comparative study of neonate and adult brain. *Biochem. J.* **395**, 417–426
62. Wei, W., Lu, Y., Hao, B., Zhang, K., Wang, Q., Miller, A. L., Zhang, L.-R., Zhang, L.-H., and Yue, J. (2015) CD38 is required for neural differentiation of mouse embryonic stem cells by modulating reactive oxygen species. *Stem Cells* **33**, 2664–2673
63. Hattori, T., Kaji, M., Ishii, H., Jureepon, R., Takarada-Iemata, M., Minh Ta, H., Manh Le, T., Konno, A., Hirai, H., Shiraishi, Y., Ozaki, N., Yamamoto, Y., Okamoto, H., Yokoyama, S., Higashida, H., Kitao, Y., and Hori, O. (2017) CD38 positively regulates postnatal development of astrocytes cell-autonomously and oligodendrocytes non-cell-autonomously. *Glia* **65**, 974–989
64. Mayo, L., Jacob-Hirsch, J., Amariglio, N., Rechavi, G., Moutin, M.-J., Lund, F. E., and Stein, R. (2008) Dual role of CD38 in microglial activation and activation-induced cell death. *J. Immunol.* **181**, 92–103
65. Wei, W.-J., Sun, H.-Y., Ting, K. Y., Zhang, L.-H., Lee, H.-C., Li, G.-R., and Yue, J. (2012) Inhibition of cardiomyocytes differentiation of mouse embryonic stem cells by CD38/cADPR/Ca2+ signaling pathway. *J. Biol. Chem.* **287**, 35599–35611
66. DeFelipe, J., and Fariñas, I. (1992) The pyramidal neuron of the cerebral cortex: morphological and chemical characteristics of the synaptic inputs. *Prog. Neurobiol.* **39**, 563–607

67. Rudebeck, P. H., Walton, M. E., Millette, B. H. P., Shirley, E., Rushworth, M. F. S., and Bannerman, D. M. (2007) Distinct contributions of frontal areas to emotion and social behaviour in the rat. *Eur. J. Neurosci.* **26**, 2315–2326
68. Wang, W.-T., Hsu, W.-Y., Chiu, Y.-C., and Liang, C.-W. (2012) The hierarchical model of social interaction anxiety and depression: the critical roles of fears of evaluation. *J. Anxiety Disord.* **26**, 215–224
69. Bruzzone, S., Verderio, C., Schenk, U., Fedele, E., Zocchi, E., Matteoli, M., and De Flora, A. (2004) Glutamate-mediated overexpression of CD38 in astrocytes cultured with neurones. *J. Neurochem.* **89**, 264–272
70. Meunier, C. N. J., Callebert, J., Cancela, J.-M., and Fossier, P. (2015) Effect of dopaminergic D1 receptors on plasticity is dependent of serotoninergic 5-HT1A receptors in L5-pyramidal neurons of the prefrontal cortex. *PLoS One* **10**, e0120286
71. Joseph, A., and Turrigiano, G. G. (2017) All for one but not one for all: excitatory synaptic scaling and intrinsic excitability are coregulated by CaMKIV, whereas inhibitory synaptic scaling is under independent control. *J. Neurosci.* **37**, 6778–6785
72. Bourgeron, T. (2009) A synaptic trek to autism. *Curr. Opin. Neurobiol.* **19**, 231–234
73. Markram, K., and Markram, H. (2010) The intense world theory - a unifying theory of the neurobiology of autism. *Front. Hum. Neurosci.* **4**, 224
74. Mitre, M., Marlin, B. J., Schiavo, J. K., Morina, E., Norden, S. E., Hackett, T. A., Aoki, C. J., Chao, M. V., and Froemke, R. C. (2016) A distributed network for social cognition enriched for oxytocin receptors. *J. Neurosci.* **36**, 2517–2535
75. Bicks, L. K., Koike, H., Akbarian, S., and Morishita, H. (2015) Prefrontal cortex and social cognition in mouse and man. *Front. Psychol.* **6**, 1805
76. Selimbeyoglu, A., Kim, C. K., Inoue, M., Lee, S. Y., Hong, A. S. O., Kauvar, I., Ramakrishnan, C., Fenno, L. E., Davidson, T. J., Wright, M., and Deisseroth, K. (2017) Modulation of prefrontal cortex excitation/inhibition balance rescues social behavior in *CNTNAP2*-deficient mice. *Sci. Transl. Med.* **9**, 6733
77. Liu, H.-X., Lopatina, O., Higashida, C., Tsuji, T., Kato, I., Takasawa, S., Okamoto, H., Yokoyama, S., and Higashida, H. (2008) Locomotor activity, ultrasonic vocalization and oxytocin levels in infant CD38 knockout mice. *Neurosci. Lett.* **448**, 67–70
78. Winslow, J. T., Hearn, E. F., Ferguson, J., Young, L. J., Matzuk, M. M., and Insel, T. R. (2000) Infant vocalization, adult aggression, and fear behavior of an oxytocin null mutant mouse. *Horm. Behav.* **37**, 145–155
79. Ko, J. (2017) Neuroanatomical substrates of rodent social behavior: the medial prefrontal cortex and its projection patterns. *Front. Neural Circuits* **11**, 41
80. Kim, S., Kim, T., Lee, H.-R., Jang, E.-H., Ryu, H.-H., Kang, M., Rah, S.-Y., Yoo, J., Lee, B., Kim, J.-I., Lim, C. S., Kim, S. J., Kim, U.-H., Lee, Y.-S., and Kaang, B.-K. (2016) Impaired learning and memory in CD38 null mutant mice. *Mol. Brain* **9**, 16
81. Clément, Y., Le Guisquet, A.-M., Venault, P., Chapouthier, G., and Belzung, C. (2009) Pharmacological alterations of anxious behaviour in mice depending on both strain and the behavioural situation. *PLoS One* **4**, e7745
82. Cambon, K., Dos-Santos Coura, R., Groc, L., Carbon, A., Weissmann, D., Changeux, J. P., Pujol, J. F., and Granon, S. (2010) Aggressive behavior during social interaction in mice is controlled by the modulation of tyrosine hydroxylase expression in the prefrontal cortex. *Neuroscience* **171**, 840–851
83. Pittaras, E., Callebert, J., Chennaoui, M., Rabat, A., and Granon, S. (2016) Individual behavioral and neurochemical markers of unadapted decision-making processes in healthy inbred mice. *Brain Struct. Funct.* **221**, 4615–4629
84. Miranda, R., Nagapin, F., Bozon, B., Laroche, S., Aubin, T., and Vaillend, C. (2015) Altered social behavior and ultrasonic communication in the dystrophin-deficient mdx mouse model of Duchenne muscular dystrophy. *Mol. Autism* **6**, 60
85. Pittaras, E. C., Faure, A., Leray, X., Moraitopoulou, E., Cressant, A., Rabat, A. A., Meunier, C., Fossier, P., and Granon, S. (2016) Neuronal nicotinic receptors are crucial for tuning of E/I balance in prelimbic cortex and for decision-making processes. *Front. Psychiatry* **7**, 171

Received for publication March 14, 2018.
Accepted for publication January 7, 2019.